ARCHIVE OF MECHANICAL ENGINEERING

DOI: 10.24425/ame.2026.12677 Early Access; pp. 1–20

Kuba KRYSZCZYŃSKI [1], Dominik WILCZYŃSKI [1], Krzysztof WAŁĘSA [1]

# Bolted joint in experimental and theoretical approaches concerning load type and friction coefficient

**Received** 18 March 2026, **Revised** 9 July 2026, **Accepted** 20 August 2026, **Published online** 19 November 2026

**Keywords:** bolt tightening process, torque–axial force relationship, friction fracture, experimental mechanics, friction coefficient

This study examines stress state in bolts during tightening, highlights discrepancy between laboratory tensile-test results and operational conditions. Although torque-controlled tightening is widely used to generate preload in bolted joints, a substantial part of the applied torque is dissipated by friction rather than transformed into useful axial force. Custom-designed test stand was developed to record axial force and tightening torque simultaneously, in two configurations: standard friction and low-friction conditions achieved with a thrust rolling bearing. The tests were carried out on M5, M6, and M8 bolts in the strength classes 4.8, 5.8, and 8.8. Additional tensile tests were performed to compare the actual strength in pure tension of the bolts with the reference values of the strength class of the technical standard. The torsional stress in the core was markedly higher under standard-friction conditions and about 60% of torque was lost on under-head friction. Reducing friction under bolt head improved axial force transfer and increased the achieved preload, with lower measured torque. Nevertheless, even in the low-friction setup, the obtained axial force remained below the expected level, in the worst case the measured preload was over 45% below expected. The measured data enabled determination of friction coefficients of $\mu = 0.205$ in the thread and $\mu = 0.221$ under bolt head in dry steel-steel contact.

## 1. Introduction

Threaded fasteners are widely used in mechanical assemblies due to their ease of installation and disassembly. The recent literature review confirms that threaded fasteners are indispensable in the aerospace and automotive industries because of

✉ Krzysztof WAŁĘSA, e-mail: krzysztof.walesa@put.poznan.pl

[1]Poznan University of Technology, Poznan, Poland



© 2026. The Author(s). This is an open-access article distributed under the terms of the Creative Commons Attribution (CC-BY 4.0, https://creativecommons.org/licenses/by/4.0/), which permits use, distribution, and reproduction in any medium, provided that the author and source are cited.

their durability, cost effectiveness and clean installation process. By optimising the design and reducing the number of bolts one can reduce the weight and cost of the system without compromising reliability [1].

The mechanical performance of these joints is significantly dependent on the applied tightening torque and the clamping force it generates. Tightening a bolt leads to combined tension and torsion, which introduces a complex state of stress in the joint.

Over many years, numerous studies have investigated the axial force and torque-tension relationship in bolted joints and the influence of these parameters on the quality of the joint. To address this, a novel 3D formulation includes the effect of nut dilation, improving the accuracy of predicted pressure distributions. As indicated in the literature, classical linear torque–preload equations often overestimate preload because they neglect the contact-related effects which include local plastic deformation and surface wear [2]. Research highlight discrepancies between theoretical torque estimations and real-world axial force outcomes due to variable friction conditions. Despite the application of popular standard torque-tightening formulas, the predictive reliability of axial force remains low without direct measurement.

A review of fatigue fracture in flange joints indicates that load amplitude depends on joint stiffness, preload and geometric imperfections. Since standard fatigue tests usually apply ideal axial loads, they often do not represent real dynamic conditions, which explains why bolt failures may occur even when design guidelines are followed [3]. A key challenge is to estimate the energy distribution during bolt tightening and determine the amount of the applied torque that goes to the clamping force. The existing standards, such as PN-EN ISO 898-1:2013 [4], focus only on the case of pure axial load. So, these standards do not consider the real combined stress state that the bolts experience during assembly.

Many publishers point to the importance of determining the friction coefficient, because it can be within a wide range between 0.04 and 1.1. Precise measurement is crucial for safety in the space industry, and so is the process of selecting connections, which is a superficially simple task, but in reality, can be a very complex and sophisticated process [5]. Experimental tests on hydraulic plug screws show that friction coefficients vary in the range of 16-18 % between dry and lubricated conditions and decrease with repeated tightening; using the broad friction ranges of preload causes errors from −15% to +86% [6].

The researchers point out that, except of using well-developed computer FEM programs, examining the friction coefficient is crucial, especially in reality, because friction is responsible for approximately 90% of torque during the tightening process. Some studies highlight that simulation and using torque wrench cannot be sufficient in the case of sophisticated constructions [7]. Finite element analyses of bolted joints are highly sensitive to mesh density: coarse meshes risk missing important phenomena, whereas fine meshes greatly increase computational cost. Consequently, numerical results must be validated experimentally to ensure that friction effects are represented accurately [8]. The research focused on friction

reveals that even a small difference in determining the friction coefficient can have a big impact on the generated axial force [9].

Other studies that have been conducted in the research on the torque-tension relationship for bolted joints pointed to the problem of torque and force distribution, investigating it by changing the friction coefficient [10]. The result was that the friction coefficient in subsequent attempts of tightening was not constant, however, the measuring method was not clearly described, and the bolts were not tested until being destroyed.

Another experimental study on the relationship between torque and axial force in threaded connections is described in the paper presenting the same idea of testing torque-preload relationship [11]. The measuring device is different than that presented below: the tightening torque is applied by a hand wrench, not automatically, and no screws were destroyed, either. One of the authors' conclusions is that self-locking torque drops significantly with the increase of the tightening times within a certain range.

Other methods of testing axial force are also used. Such is the ultrasonic method [12], but it requires a specific material, and the force cannot be measured during tightening. The Digital Image Correlation method is becoming more popular in application to preload monitoring [13], but this method works well only when material parameters are known exactly.

Another research indicates that there is still a need to measure method parameters such as the speed of tightening [14]. This parameter can indirectly influence the clamping force. Recent research on nonlinear phenomena in threaded connections applies data-driven methods for axial force prediction; however, the reported experimental setup does not allow for independent control of under-head friction conditions. Using a machine-learning approach based on experimental data allows for predicting the axial force with an accuracy of up to 98%; however, the engineering applicability of such methods depends on the availability and quality of experimental data for training and validation. It shows that there is the need to further develop and expand experimental research in this area [15]. A similar study has also combined experimental data with a feed-forward neural network to predict bolt capacity and friction coefficients. By capturing nonlinear correlations, the presented model achieved an accuracy of over 95% [16]. This showed that machine learning approaches could complement traditional torque–preload methods, so they are becoming more popular. In the context of modern industrial production, some authors propose a tightening method based on augmented reality and a tracked connected torque wrench. The system assists the operator during tightening, ensures that each bolt reaches the required torque and automatically records the process, which improves assembly reliability and reduces human error [17].

Although torque-preload correlation, friction variability, and preload monitoring have been studied for years, there is still a considerable gap in experimental data. In many studies, friction is treated as an assumed input or is identified indirectly, while analysis often focuses mainly on preload prediction without clearly

separating the effects that occur in the threads from those under the bolt head during tightening [14–16]. At the same time, although numerical models can capture general trends, their outcomes strongly depend on the choice of modelling methods and contact assumptions, so they still need solid experimental validation. For this reason, the torque partitioning and the resulting axial stress state under different, controlled under-head friction conditions are not sufficiently quantified, especially in a way that can be directly compared with standardised tensile test results and used to assess how far the simplified torque formulas can be trusted.

The purpose of this study is to investigate the behaviour of bolts under practical tightening conditions and to compare the response of the tested bolts with the results of standardised tensile tests [18] under different under-head friction conditions. The study includes experimental tightening tests performed using various friction configurations, as well as additional tensile tests carried out according to the PN-EN ISO 6892-1:2020 [18]. For this purpose, a dedicated experimental stand was designed, manufactured and used. This custom stand allows one to set friction coefficient and apply methods that can help improving other testing methods known from the literature. The stand then helps to fill the research gap by enabling a simultaneous measurement of torque and axial force during tightening.

## 2. Methods and materials

The tests were performed using a custom-designed measuring test stand that enables simultaneous acquisition of tightening torque ($M$) and axial force ($F$) (Fig. 1).

The stand is vertically mounted (Fig. 1). From the top, a BLDC motor (1) with a planetary gearbox (2) is used; the output torque can reach 70 Nm. The drivetrain consists of a torque transducer (4) connected by two jaw couplings, followed by a movable shaft and socket (6, 7). These components are responsible for applying and measuring the tightening torque. The lower part of the assembly, shown in Fig. 1 (details A and A′), is responsible for measuring the axial force generated in the bolted joint. The main element is a piezoelectric force sensor (14) with a range of up to 80 kN and high stiffness compared to overall joint compliance. Between the sensor and the under-head support sleeve (10), two alternative elements can be installed: a thrust rolling bearing (11) or a support sleeve (12). All components were designed to be compact and tightly fitted in order to maximise stiffness and minimise parasitic deformation.

The stand used in this study (Fig. 1) allows one to measure the influence of many parameters such as: speed of tightening, temperature, type and amount of lubrication, type of friction under-head, number of screw tightening cycles. All of the above parameters can be changed separably, which gives the possibility to exactly determine how these parameters influence the generated axial force and the tightening torque.

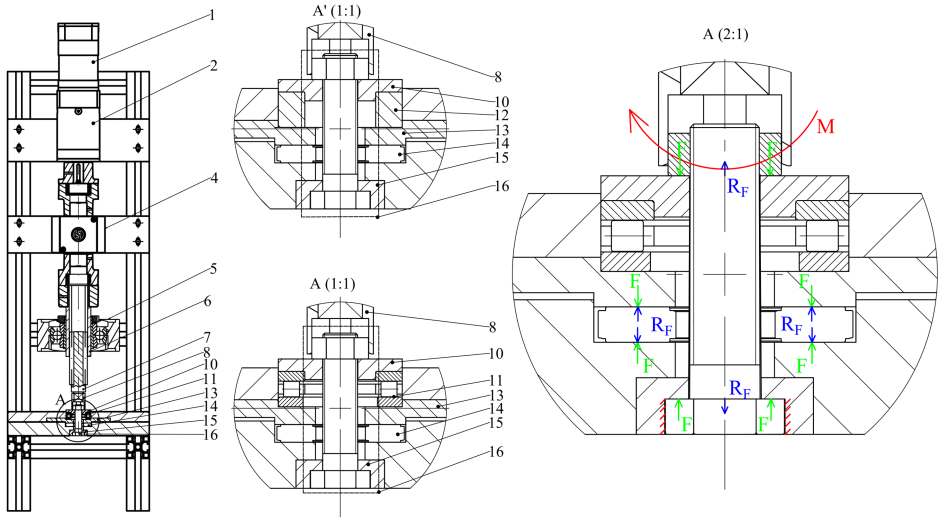



Fig. 1. Test stand – technical drawing key parts: 1 – motor, 2 – planetary transmission, 4 – torque metre, 5 – bearing, 6 and 7 – movable shaft, 8 – socket, 10 – under-head support, 11 – thrust bearing, detail A (or 12 – support sleeve – detail A′), 13 – transfer plate, 14 – force sensor, 15 – nut holder, 16 – tested screw connection, right part: $M$ – measured torque, $F$ – axial force, $R_F$ – reaction force

This setup enables observation of the points at which the torque and the axial force attain a peak and how they relate over the course of tightening. The tightening speed is constant in all configurations and equal to 5 rpm. This corresponds to a thread advance rate of $v = n \cdot p$, approximately 4–6.25 mm/min depending on the pitch of the thread, and this is the kinematic advance of the thread; the actual elongation of the bolt depends on the joint force-stiffness response. This value is in the speed range in the steel static tensile test [18]. The sampling frequency is set to 5 Hz, allowing real-time acquisition of force and torque in a synchronised manner. At 5 rpm (12 s/rev), this corresponds to approximately 60 samples per revolution, which is sufficient to capture the evolution and peaks of both signals and to ensure a reliable relationship between force and torque changes. To allow for comparison of results, all bolts were tested under the same conditions, including temperature (20°C) and consistent surface condition received. No additional lubrication or cleaning was applied beyond the factory condition, to imitate typical non-dynamic application conditions.

Each group consisted of bolts of a given size, strength class, and friction configuration, with 5–10 samples per group. In total, 18 groups were tested, covering all combinations of three bolt sizes (M5, M6, M8), three strength classes (4.8, 5.8, 8.8), and two friction configurations (standard friction, Fig. 1 A′, and low under-head friction using a thrust bearing, Fig. 1 A). The torque can be applied to the screw head or to a nut; in this study, the torque was applied to the screw head.

The setup was configured in two primary configurations:

- standard configuration with friction under the bolt head due to steel–steel contact (Fig. 1, detail A′),
- low-friction configuration using a thrust bearing under the head to reduce the friction contribution of the under-head to the torque [19] (Fig. 1, A).

Additionally, tensile tests were carried out on an MTS 50 kN universal testing machine according to PN-EN ISO 6892-1:2020 [18] (Fig. 2). These tests were used to track changes in axial stress at pure tensile loading. A constant crosshead displacement rate of 6 mm/min was applied, which was similar to the deformation speed during tightening of the joint on the stand (Fig. 1) and was consistent with the standard of static tensile testing [18]. In each group tested, at least 3 screws were tested; the scatter of tensile results was low (below 3% relative to the group average). The analysis was focused only on the ultimate tensile strength $R_m$. Yield strength $R_e$ was not considered, as the onset of yielding was often gradual and difficult to identify.

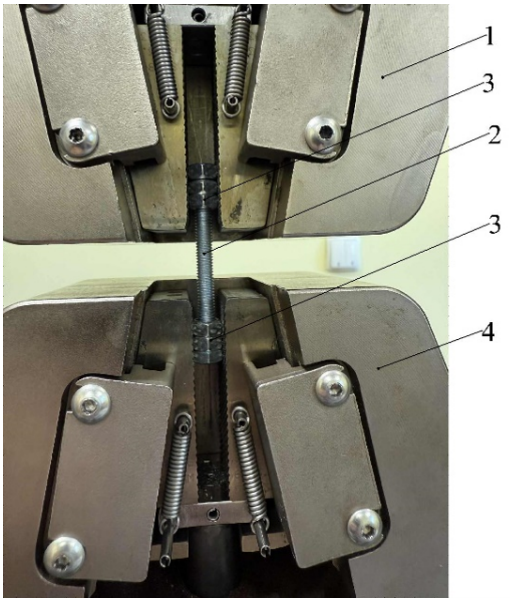



Fig. 2. MTS clamp tested screw – technical drawing key parts:
1 – movable clamp, 2 – tested screw, 3 – high nut, 4 – fixed clamp

The aim of the present study is not to replace the standardised bolt testing procedure described in PN-EN ISO 898-1 [4]. Instead, the proposed approach was used to analyse the behaviour of the joint during tightening, where torque, axial force, and friction-related effects occur simultaneously. This makes it possible to obtain additional information about the real load state of the joint, beyond that provided by standard tensile testing alone. The result of this test can be used to compare with the strength class value and as a reference point to the load state under real conditions.

## 3. Results and discussion

### 3.1. General observations

The photograph of selected bolts after testing is presented in Fig. 3. There is not any clear trend, related to bolt size, that one can visually notice. However, one can observe some differences between the test configurations and the strength class.

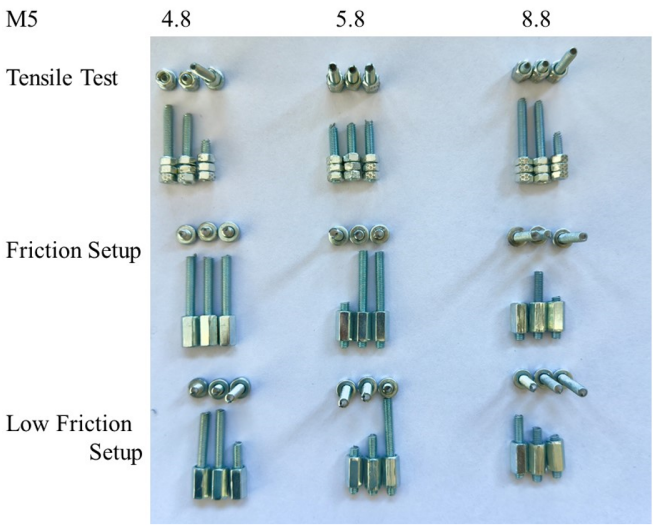



Fig. 3. Selected bolts after testing

In both configurations on the test stand, a qualitative trend was observed. The strength class appeared to influence the location of the fracture. In lower classes, such as 4.8, the fracture generally appeared closer to the head where the tightening torque was applied. In higher classes, e.g. 8.8, the fracture was more often located closer to fixed end. This observation may indicate that lower-strength bolts, which undergo greater plastic deformation before fracture, may be more influenced by the side of torque application, while higher-strength bolts may be more sensitive to local stress concentration near the fixed end.

The location of the fracture and the visibility of the neck were related to the type of test. After tensile tests, the fracture usually occurred in the middle part of the bolt, between the head and the nut, and the neck was visible. In the high friction configuration, the fracture was more often located close to the head or the nut, while the fracture in the middle part of the bolt was less frequent, as if in this configuration the neck was not significant. In the low under-head friction configuration, the necking was not significant, either, while the fracture location was more scattered and usually was not located directly next to the head or the nut. However, if the torsion takes the largest part, it is more likely that the fracture

occurs closer to the one of the constrained ends. This qualitative tendency in the type and location of the fracture can be treated as a preliminary finding, so more research with simple stress states, and then with complex stress states is needed to give clear conclusions.

The test stand records data from two sensors: the axial force value and the torque value. Both signals are recorded as functions of time and can therefore be presented separately in time-based plots. However, when the axial force is plotted as a function of the tightening torque, the mechanical response of the bolt during tightening becomes clearer. This form of presentation makes it possible to observe how the axial force develops with increasing torque (Fig. 4). This type of plot reveals directly the relationship between force and torque, and better shows the crucial non-linear final part. The blue part represents the growth of force, and the red part represents the decrease of force. The plot clearly reveals the course of the applied load: the initial portion of the curve is nearly linear, after reaching a peak value the force drops, which typically corresponds to thread stripping or plastic deformation of the shank. The moment of maximum axial force and maximum torque is crucial. It reveals the critical area where the torque is still rising but the axial force drops (red part). It can be caused by a significant plastic elongation of the bolt core, leading to a mismatch of the threads in the bolt and the nut. This process causes that an additional source of friction appears, significantly reducing the efficiency of the threaded connection.

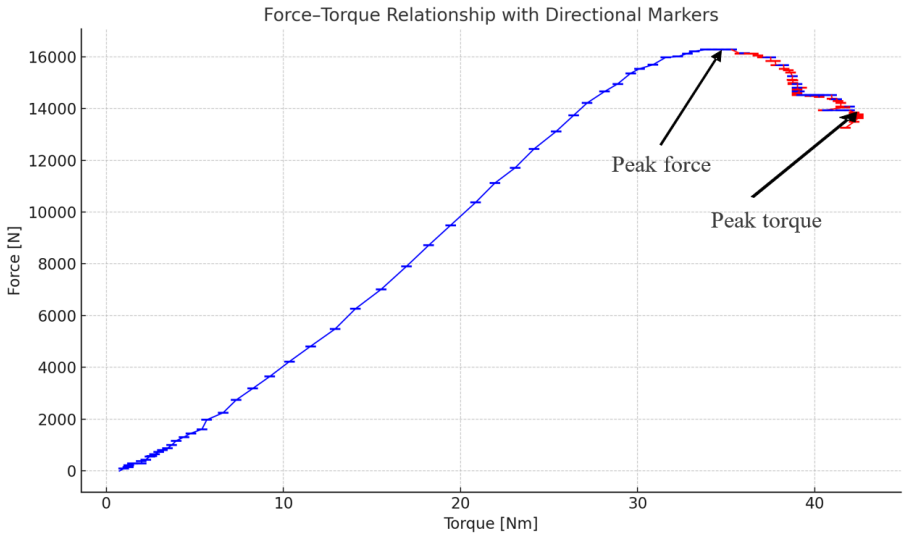



Fig. 4. Exemplary force-torque plot, screw M6 8.8

Other researchers note that such local plasticity increases the effective contact area and friction at the thread interface, altering the torque-force path. This corresponds to the non-linear red segment observed in the plot, where additional torque

is required to maintain rotation even though the net axial force decreases [20]. Another paper with FEM analyses shows that under high preload conditions shear stresses at the root of the thread and the surface of the thread increase, potentially leading to local yielding before complete tensile failure of the shank [21]. In the force-torque plot, this would appear in the red part region, where the torque continues to increase, but the effective axial tension drops due to plastic shear redistribution (Fig. 4).

From a mechanical point of view, the post-peak part of the torque-axial force curve may correspond to the onset of local instability within the threaded engagement. The authors of [22] demonstrated that once the neck develops near the nut, the engaged bolt threads are displaced radially inward, the thread overlap is reduced, and the first engaged threads may become disengaged (Fig. 5, bottom [22]). The load is then transferred to fewer active threads, which intensifies local bending stress, shear stress, and friction-related shear effects as a part internal effects inside the material, and additionally normal contact pressure between the remaining

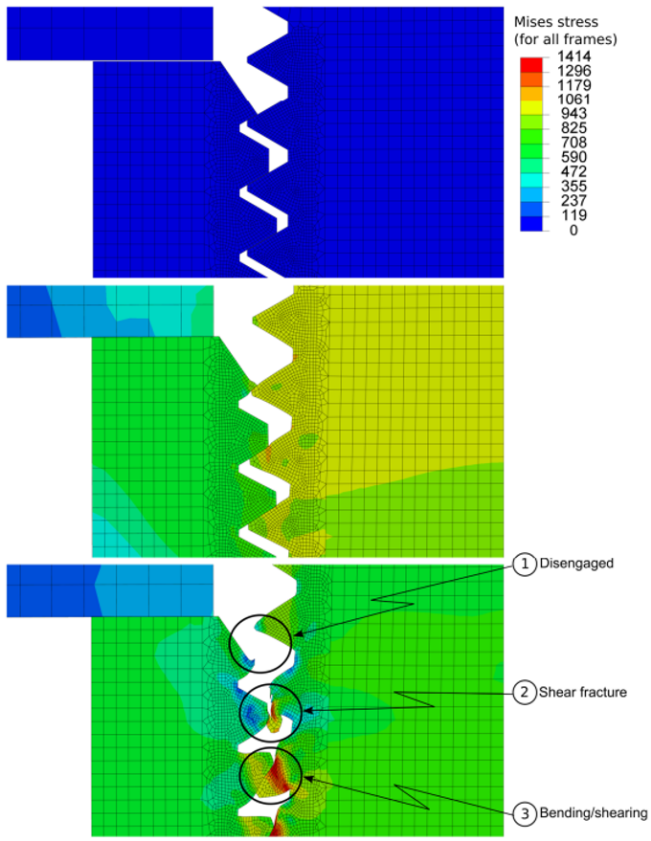



Fig. 5. Literature-based numerical example of progressive thread degradation reported in [22]: undeformed state, initiation of yielding, and thread failure

thread flanks. This mechanism explains why additional torque may still be required to maintain rotation even though the net axial force decreases: the connection no longer functions as an efficient preloading system, but increasingly as a locally damaged contact system with deteriorating thread engagement [22]. It should be emphasised that Fig. 5 presents a numerical example based on the mentioned literature on progressive thread degradation. In the present tests, the failure usually occurred caused by the fracture of the bolt core before a complete destruction of the engaged threads developed.

### 3.2. Axial stress calculations

The axial stress was calculated using the standard engineering equation (1):

$$\sigma_a = \frac{F}{A_s}, \tag{1}$$

where: $F$ – axial force [N], $A_s$ – effective tensile stress area [mm$^2$], taken from PN-EN ISO 898-1:2013 [4].

The stress area $A_s$ reflects the effective load-carrying profile of the thread. It was calculated using an effective diameter $d_s$ defined as the average diameter of $d_1$ basic minor diameter thread and $d_2$ basic pitch diameter (Fig. 6). To clarify this point, cross-section of the bolt is always larger than the core area alone, because a part of the thread is present in the cross-section. The area calculated from the diameter of the core $d_1$ may be sufficient for simplified engineering calculations, but it does not accurately represent the effective load-carrying area of the threaded section. Using only the diameter of the core would overestimate stress [4].

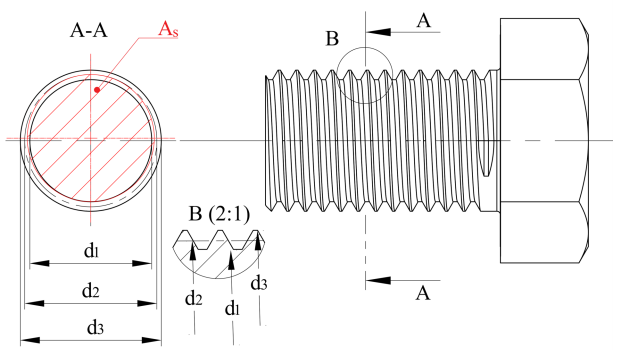



Fig. 6. ross-section of the screw with effective tensile stress area

Three values of axial force were considered:

- from tightening with under-head friction (steel-steel contact) (Fig. 1, detail A′),
- from tightening with a low-friction bearing setup (Fig. 1, detail A),
- from standard tensile testing on an MTS 50 kN machine (Fig. 2).

Fig. 7 presents the average values of axial stress in [MPa] calculated from the measured maximal force values. The blue bar represents the experimental result of the MTS Insight Electromechanical 50 kN tensile testing machine, the other two bars show the stress of the generated axial force measured on the custom test stand, while the torsional stress was neglected. The yellow bar shows the standard friction setup (Fig. 1, detail A′), while the green bar illustrates the low friction setup (Fig. 1, detail A). The red horizontal lines in the graph indicate the theoretical ultimate tensile strength $R_m$, according to the relevant strength class [4]. As a reference point, the lowest force value was 6398 N for M5, 4.8 class, and the highest was 20 979 N for an M6 class 8.8 bolt. These results are presented in Fig. 7 transformed into axial stress values, instead of force values, to unify the results across bolt sizes. The graph reveals that not all the screws withstand the minimum required axial force, even when measured under pure tensile loading. M6 4.8 and M5 8.8 do not meet the standard requirements. However, the screws M5 5.8 exceed the theoretical minimum by more than 45%, which means a significant stress dispersion in the results; the remaining M5 4.8, M6 5.8, M6 8.8 meet the standard. All the bolts tested on the custom-designed stand under torque exhibit axial stresses below the minimum specified by the standard for axial force. This led to further analysis of torsional stress levels in the bolted connection. However, it is difficult to identify any consistent trend or correlation between them. The measured values appear highly scattered, with no clear correlation, suggesting a random character of the results. The static tensile tests did not include bolts size M8 due to the excessively high axial forces that would exceed the load capacity of the testing machine and create a risk of local surface pressure issues. Therefore, only the bolts of size M5 and M6 were tested.

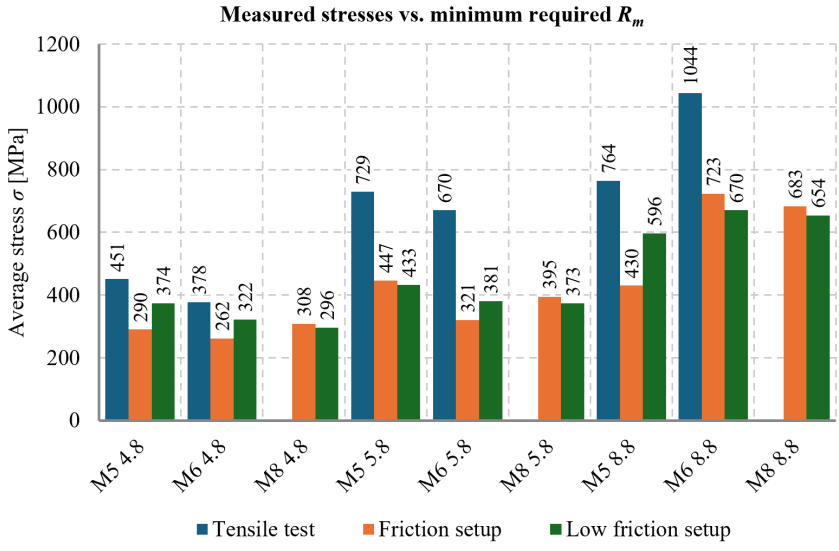



Fig. 7. Comparison of axial stress with standard requirements

### 3.3. Torque and friction analysis

Measurement of the tightening torque and the axial force was performed in two configurations, with high and low under-head friction. This created the possibility to define the friction coefficient and differentiate friction coefficients in threads and under-head. It was done in two steps. Firstly, equation (2) [25] was introduced, and the standard engineering formula was used to calculate the required tightening torque:

$$M = F\left(\frac{d_2}{2}\tan(\gamma+\rho') + \frac{D_h}{2}\mu\right), \tag{2}$$

where: $M$ – tightening torque [Nm], $F$ – axial force [N], $d_2$ – effective pitch diameter [m], $D_h$ – average diameter of the contact area under the head [m], $\gamma$ – helix angle [°], $\rho'$ – apparent friction angle [°], $\mu$ – coefficient of friction.

In equation (2), there are two friction coefficients, one in the thread (as the friction angle) and the second one is the under-head coefficient of friction. In the first step, a simplification was introduced by assuming the same friction coefficients in both contact regions. Equation (2) was transformed to determine the equivalent coefficient of friction (Eq. (3)):

$$\mu = \frac{d_2 + D_h\cos\alpha + \dfrac{2M}{F}\tan\gamma}{2D_h\tan\gamma} - \frac{\sqrt{\left(d_2 + D_h\cos\alpha + \dfrac{2M}{F}\tan\gamma\right)^2 - 4D_h\cos\alpha\tan\gamma\left(\dfrac{2M}{F} - d_2\tan\gamma\right)}}{2D_h\tan\gamma}. \tag{3}$$

The torque and force values were taken from the high friction configuration, assuming that friction should be similar in both contact areas. The outcome of this calculation is in Table 1, and the average coefficient of friction $\mu = 0.205$. This is a value very close to the commonly assumed value for steel-steel contact ($\mu = 0.2$) [23].

Table 1. Coefficients of friction determined in the approach (from Eq. (3))

| Size | Class | | | |
|---|---|---|---|---|
| | M5 | M6 | M8 | Average |
| 4.8 | 0.169 | 0.156 | 0.213 | 0.179 |
| 5.8 | 0.294 | 0.214 | 0.239 | 0.249 |
| 8.8 | 0.179 | 0.182 | 0.199 | 0.187 |
| Average | 0.214 | 0.184 | 0.217 | 0.205 |

In the second step we aimed to achieve different coefficients of friction in the thread and under-head in both configurations (high and low friction). Equa-

tion (2) was transformed again without simplification, designating the under-head coefficient of friction:

$$\mu = \frac{2M}{F\,D_h} - \left(\frac{d_2}{D_h}\tan(\gamma + \rho')\right). \tag{4}$$

The friction coefficients $\mu$ calculated above (Table 1) were transformed to the friction angle $\rho'$ and these values were substituted into Equation (4), taking exact values for each size and strength class. The values in Tables 2 and 3 are calculated using this formula. For example, the average value of the coefficient of friction $\mu = 0.205$ corresponds to the angle of friction $\rho' = 13.31^\circ$.

Table 2. Coefficients of friction under the head (high friction)

| Size | Class | | | |
|---|---|---|---|---|
| | M5 | M6 | M8 | Average |
| 4.8 | 0.195 | 0.192 | 0.192 | 0.193 |
| 5.8 | 0.271 | 0.302 | 0.225 | 0.266 |
| 8.8 | 0.302 | 0.132 | 0.177 | 0.204 |
| Average | 0.256 | 0.209 | 0.198 | 0.221 |

Table 3. Coefficients of friction under the head with the bearing (low friction)

| Size | Class | | | |
|---|---|---|---|---|
| | M5 | M6 | M8 | Average |
| 4.8 | 0.085 | 0.095 | 0.111 | 0.097 |
| 5.8 | 0.215 | 0.160 | 0.142 | 0.173 |
| 8.8 | 0.153 | 0.129 | 0.108 | 0.130 |
| Average | 0.151 | 0.128 | 0.121 | 0.133 |

The values in Table 2 can be treated as reference parameters. The percentage difference is 7.8% between the average under-head friction $\mu = 0.221$ and the substituted value $\mu = 0.205$. This is not the perfect one, but the best possible way to differentiate frictions. To minimize the error, a new value can be substituted in Formula (3).

In Table 3, there are the compiled values of the coefficient of friction under the head in the bearing configuration. The values are high, as for typical thrust bearings, which is caused by poor lubrication of the bearing. If the bearing was properly lubricated, the lubricant could spread to the tested screw and influence the friction in the thread. The friction value in the sliding friction range for steel-steel contact is (0.08–0.2) [19]. However, the friction under the head is still reduced almost by half compared to that in steel-steel contact.

It should be noted that the friction coefficient value will not be constant during the tightening process due to the forces close to flow stress which cause smoothing or lapping. This is not always desirable, because it can lead to self-unscrewing and, furthermore, a screw once used should not be used again.

Fig. 8 is a graphic representation of Tables 1, 2, and 3. The values from Table 1 are the dark blue bars representing the friction coefficient calculated in the simplified method which employs the averaged value of friction under the head in high-friction configuration and the friction in threads. The values from Table 2, plotted as orange bars, are the recalculated values of the coefficient of friction at the surface located under the head of the bolt (steel-steel contact) under real conditions. Finally, Table 3 is represented by pink bars, pertaining to the minimised friction under-head.

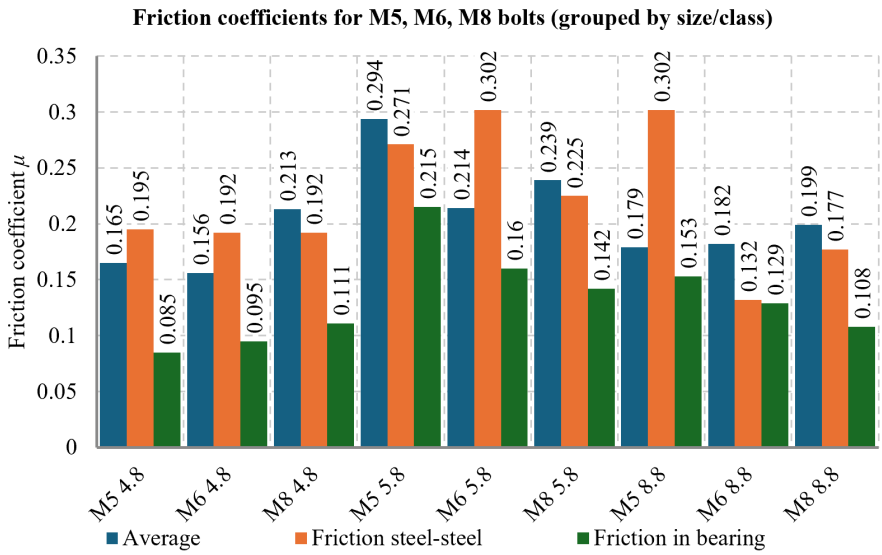



Fig. 8. Coefficients of friction under-head in high- and low friction configurations

The trend visible in the tables is that larger screws generate lower friction under the head. However, the geometry of screws, especially the $A_B$ under-head area, is not growing linearly with the axial force ratio of the under-head surface to the $A_S$ effective tensile stress area, it is 0.96 for M5, 1.39 for M5 and 1.15 for M8 (Table 4). Theoretically, the surface of contact does not influence friction; however, it can influence the surface structure and the processes such as lapping and smoothing of the under-head area. The influence of pressure on the friction coefficient may be negligible at low contact stress levels. However, when the pressure is high and approaches the limit of the surface pressure of the material, it may significantly affect friction conditions. The under-head pressure is different in each group tested; this fact can be one of the causes for high scatter of results (Fig. 8).

Table 4. Ratio of the under-head area $A_B$ to effective tensile stress area $A_S$

| Bolt size | $A_s$ [mm$^2$] | $A_b$ [mm$^2$] | $A_b/A_s$ |
|---|---|---|---|
| M5 | 14.2 | 13.6 | 0.958 |
| M6 | 20.1 | 28 | 1.39 |
| M8 | 36.6 | 42.1 | 1.15 |

The other quantity is friction, in all configurations, which takes the biggest value in 5.8 class and is lower in other classes. It is theoretically known that the higher the hardness, the lower the friction should appear, and this information can be found in many research articles on the coefficient of friction of steel [26]. It is difficult to explain why friction is the lowest in the 4.8 class. It is possible that due to very low hardness some borderline phenomenon appears. This hypothesis was formulated in other research. The tests on M10-M20 bolts show that bolt diameter, wrench power, and socket length markedly influence thread and bearing friction; smaller bolts exhibit higher friction and scatter, and these effects are not yet fully captured in the current models [26].

In Fig. 8, there is a summary of Tables 1, 2, and 3. The highest values pertain to the screws of class 5.8. However, there are not any purely visible trends; the values are mostly scattered. One can assume that, if the calculated friction under-head was lower, than the value calculated from equation (3), the friction in threats, would be slightly higher than that in Table 1. However, in the opposite case, if the calculated friction under-head was higher, the friction in threats should be a little lower than that in Table 1.

### 3.4. Torque contribution

In this analysis, it is assumed that the total torque $M$ consists of two primary components due to friction [14]:

$$M = M_t + M_h\,, \tag{5}$$

$$M_t = F\frac{d_2}{2}\tan(\rho' + \gamma), \tag{5a}$$

$$M_h = \frac{D_h}{2}F\mu'_h\,. \tag{5b}$$

Equation (5a) represents the torque from thread friction and Eq. (5a) represents the torque from the under-head (bearing surface) friction.

In the previous section, the friction coefficient values were calculated, and now using those values and the above formulas it is possible to define torque utilised in the thread and under-head. The sum of $M_t$ and $M_h$ (Eq. (5)) is the value measured on the torquemeter. It gives the possibility to show the distribution of the torque.

Fig. 9 is a representation of the torque distribution. The whole height of a bar is the total torque that is measured on the stand. For each screw, there are two bars for the low (blue) and high (green) friction configuration. The lower bar (dark blue and dark green) represents the under-head part. The upper part of a bar (light blue and light green) is the torque consumed on thread friction. An additional representation of Fig. 9 is Fig. 10, and the only difference between them is that the total torque is represented as 100% and the under-head and thread parts are represented as two parts of the bar.

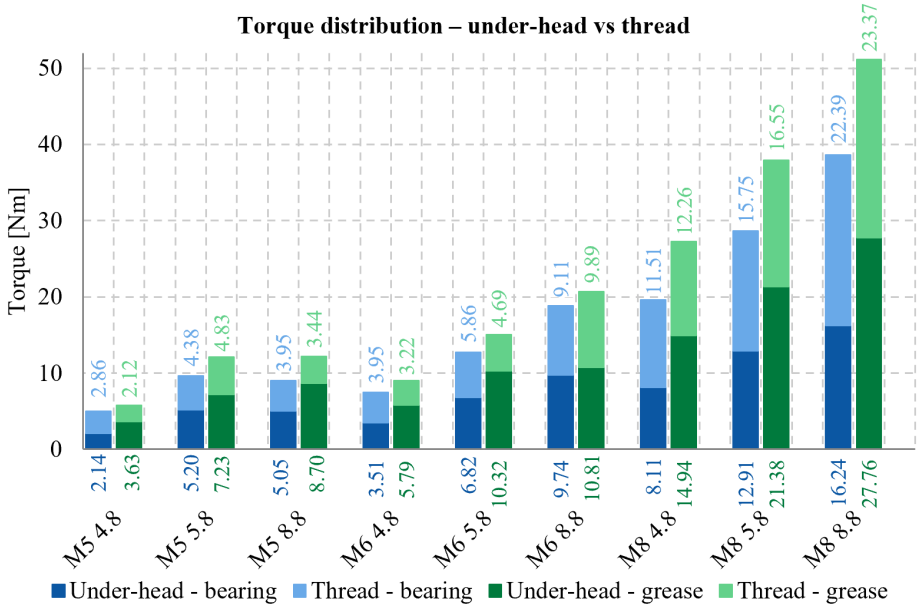



Fig. 9. Torque distribution on friction under-head and in threads during tightening

Fig. 9 shows that for each case in high friction configuration a higher torque is required to destroy the connection. However, comparing it with Fig. 7 one can see that usually low friction configuration generates a higher axial force. There are two reasons for this effect. First, with lower friction under-head a smaller torque is needed to generate the same axial force, and second, the greater the torque under-head, the larger the contribution of torsional stress, which weakens the connection.

In high friction configuration, one can see that the part of under-head torque reaches more than 60% (Fig. 10), which leads to the increase of axial force in low friction configuration (Fig. 7). So that, under-head friction can influence the distribution of torque, which is commonly known, but it can also influence the maximal axial force of the bolt. This effect should be taken into account when considering the bolt ultimate tensile capacity.

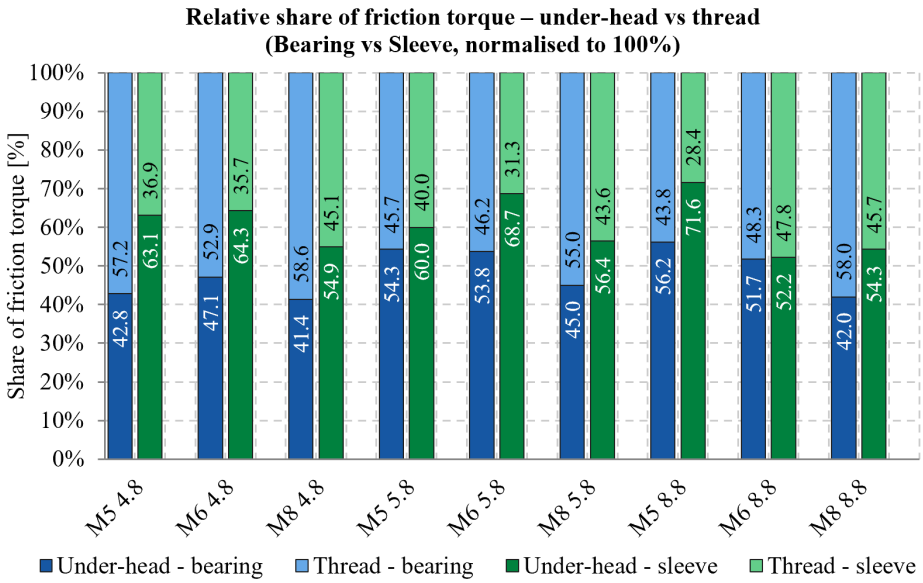



Fig. 10. Torque distribution on friction under-head and in threads during tightening as share

## 4. Concluding remarks

The subject of this research was the bolt joint analysed in experimental and theoretical approaches with respect to the type of load and the friction coefficient. Bolt joints are popular in many fields of mechanical engineering, and their mechanical properties are widely known. However, a research gap still exists in this field, especially due to the development of new measurement methods, new materials and new applications.

The main difficulty of this research is the complex nature of the tightening process. It is due to the fact that several parameters change simultaneously, and it is almost impossible to represent them as linear functions to simplify relationships. Other parameters, such as stiffness of the testing devices also create problems, because there are not any perfectly rigid materials. Contrary to FE methods, where elements not directly involved in the test are usually assumed perfectly rigid, in experimental tests it is not possible, and this will always be a source of error when comparing results of these two methods of testing. The data collected from the test stand is a source of information for machine learning and artificial intelligence programmes allowing accurately simulate the actual operational conditions.

The research gap is still present in the area such as tribological analysis of contact threads, especially using FE methods. Although simulation results are very good in linear ranges of material properties, errors increase significantly after exceeding the linear range [27]. A major advantage of the developed test stand is

the possibility of measuring the whole load range, from a zero load to the fracture of the tested bolt. This allows one to analyse non-linear, near-fracture phenomena.

Further theoretical mechanical analysis of the fracture sites can be conducted to define, for example, the relationship between fracture location and material properties or distribution of forces. Some observations have been made, however, they only allow for preliminary conclusions. This type of research could be useful for investigating the causes of accidents [28, 29].

This research shows how significant and complex is the friction under-head. In the case of force distribution, it is recommended to reduce this friction in order to generate a greater axial force. It can be achieved by using a low-friction washer. On the other hand, higher friction under the head prevents self-unscrewing. This principle is used in wedge-locking washers. A synergic combination of these two features should be tested on a test stand, such as the one developed in this research.

The test stand presented in this study made it possible to determine the operational clamping force and allowed for drawing some interesting conclusions, e.g., that under favourable friction conditions, some bolts generate an axial force close to the value expected from their strength class. In contrast, some bolts tested without influencing friction generated only about 50% of the theoretically expected axial force. This test stand gives the possibility to conduct further tests of screw joint in operational conditions. It makes it possible to determine: the coefficient of friction, the maximal axial force, the effective clamping force and the tightening torque to make a reliable joint. Furthermore, it enables measurements, in a repeatable way, of the influence of parameters such as washer type, lubrication of a thread and the structure of surface area of the thread.

## References

[1] D. Croccolo, M. De Agostinis, S. Fini, M.Y. Khan, M. Mele, and G. Olmi. Optimization of bolted joints: a literature review. *Metals*, 13(10):1708, 2023. doi: 10.3390/met13101708.

[2] J. Zhang, J. Feng, W. Li, and R. Liao. Improving torque-tension relationship in bolted joints: accurate threaded surface representation and pressure distribution considerations. *Mechanics Based Design of Structures and Machines*, 52(10):7705–7725, 2024. doi: 10.1080/15397734.2024.2308648.

[3] I. Okorn, M. Nagode, J. Klemenc, and S. Oman. Examining the effects on a fatigue life of preloaded bolts in flange joints: an overview. *Metals*, 14(8):883, 2024. doi: 10.3390/met14080883.

[4] PN-EN ISO 898-1:2013. Mechanical properties of fasteners made of carbon steel and alloy steel – Part 1: Bolts, screws and studs with specified property classes – Coarse thread and fine pitch thread. Polish Committee for Standardization, Warsaw, 2013.

[5] R.T. Barrett. *Fastener Design Manual*. NASA Reference Publication 1228, National Aeronautics and Space Administration, Washington, D.C., 1990.

[6] J. Hladnik, F. Majdič, A. Čelik, and B. Jerman. Dependence of the preload on the tightening torque for hydraulic plugs. *Applied Sciences*, 14(24):11920, 2024. doi: 10.3390/app142411920.

[7] R.I. Rousseau and A.-H. Bouzid. The tightening and untightening modeling and simulation of bolted joints. *Machines*, 12(9):654, 2024. doi: 10.3390/machines12090654.

[8] M. Zhang, D. Zeng, L. Lu, Y. Zhang, J. Wang, and J. Xu. Finite element modelling and experimental validation of bolt loosening due to thread wear under transverse cyclic loading. *Engineering Failure Analysis*, 104:341–353, 2019. doi: 10.1016/j.engfailanal.2019.05.001.

[9] S.A. Nassar, P.H. Matin, and G.C. Barber. Thread friction torque in bolted joints. *Journal of Pressure Vessel Technology*, 127(4):387–393, 2005. doi: 10.1115/1.2042474.

[10] Y. Jiang, J. Chang, and C.-H. Lee. An experimental study of the torque-tension relationship for bolted joints. *International Journal of Materials and Product Technology*, 16(4–5):417–429, 2001. doi: 10.1504/IJMPT.2001.001264.

[11] Q.M. Yu, X.J. Yang, and H.L. Zhou. An experimental study on the relationship between torque and preload of threaded connections. *Advances in Mechanical Engineering*, 10(8):1–10, 2018. doi: 10.1177/1687814018797033.

[12] G. Ren, H. Zhan, Z. Liu, W. Jiang, R. Li, and S. Liu. Evaluation of axial preload in different-frequency smart bolts by laser ultrasound. *Sensors*, 22(22):8665, 2022. doi: 10.3390/s22228665.

[13] L. Huo, L. Zhao, A. Hu, F. Meng, and H. Li. Digital image correlation-based bolt preload monitoring. *Sensors*, 26(3):913, 2026. doi: 10.3390/s26030913.

[14] E.V. Persson, M. Kumar, C. Friberg, and N. Dressler. Clamp force accuracy in threaded fastener joints using different torque control tightening strategies. *SAE Technical Paper*, 2021-01-5073, 2021. doi: 10.4271/2021-01-5073.

[15] Y. Qiao, B. Zhao, D. Deng, and W. Ouyang. Prediction model for nonlinear variation of bolt preload with tightening torque based on mechanism and data fusion. *Scientific Reports*, 15:8020, 2025. doi: 10.1038/s41598-025-88213-y.

[16] I. Boujnah, N. Afifi, A. Wettstein, and S. Matthiesen. Towards precision in bolted joint design: a preliminary machine learning-based parameter prediction. *Proceedings of the Design Society*, 5:3211–3220, 2025. doi: 10.1017/pds.2025.10335.

[17] A. Fau, M. Ghobrial, P. Seitier, P. Lagarrigue, M. Galaup, A. Daidié, and P. Gilles. Enhancing performance in bolt torque tightening using a connected torque wrench and augmented reality. *arXiv*, 2025. doi: 10.48550/arXiv.2505.10047.

[18] PN-EN ISO 6892-1:2020. Metallic materials – Tensile testing – Part 1: Method of test at room temperature. Polish Committee for Standardization, Warsaw, 2020.

[19] SKF. *Łożyska toczne*. PUB BU/P1 10000 PL, SKF, 2014. Available at: https://cdn.skfmediahub.skf.com/api/public/0901d1968037429b/pdf_preview_medium/0901d1968037429b_pdf_preview_medium.pdf, accessed 15 July 2025.

[20] G.E. Dieter. *Mechanical Metallurgy*. 3rd ed., McGraw-Hill, New York, 1986.

[21] Q.M. Yu, H. Zhou, and L. Wang. Finite element analysis of relationship between tightening torque and initial load of bolted connections. *Advances in Mechanical Engineering*, 7(5):1–8, 2015. doi: 10.1177/1687814015588477.

[22] E.L. Grimsmo, A. Aalberg, M. Langseth, and A.H. Clausen. Failure modes of bolt and nut assemblies under tensile loading. *Journal of Constructional Steel Research*, 126:15–25, 2016. doi: 10.1016/j.jcsr.2016.06.023.

[23] W. Skotnicki, D. Jędrzejczyk, and I. Szłapa. Comparative study of zinc coatings tribological properties in a dry friction conditions. *Proceedings of the 25th Anniversary International Conference on Metallurgy and Materials*, 977–982, Brno, Czech Republic, 2016.

[24] T. Kretschmer, M. Doellken, P. Haberkern, N. Frank, F. Leitenberger, A. Albers, and S. Matthiesen. Frictional behavior of bolted joints during impact tightening. *Discover Applied Sciences*, 8:152, 2026. doi: 10.1007/s42452-026-08273-1.

[25] J.H. Bickford. *Introduction to the Design and Behavior of Bolted Joints: Non-Gasketed Joints*. 4th ed., CRC Press, Boca Raton, FL, 2007.

[26] M.O.A. Mokhtar. The effect of hardness on the frictional behaviour of metals. *Wear*, 78(3):297–304, 1982. doi: 10.1016/0043-1648(82)90240-X.

[27] R. Nykänen. *Simulation of Bolted Joint with Frictional Contacts*. MSc thesis, Luleå University of Technology, Luleå, Sweden, 2019.

[28] L. Chen, Y. Feng, and K. Ding. Research on corrosion fatigue fracture mechanism and failure analysis of aircraft main wheel hub bolts. *Journal of Physics: Conference Series*, 3098(1):012018, 2025. doi: 10.1088/1742-6596/3098/1/012018.

[29] Aeroengine Safety. Failures of bolts and nuts. Institute of Thermal Turbomachinery and Machine Dynamics, Graz University of Technology. Available at: https://aeroenginesafety.tugraz.at/doku.php?id=23:233:2331:23312:23312, accessed 8 June 2026.